IRSTI 29.05.45 https://doi.org/10.26577/ijmph.2024v15i1a7

Ye. Kurmanov[1,2,3*], T. Konysbayev[1,2], G. Suliyeva[1,2,4], G. Ikhsan[1], N. Saiyp[2], G. Rabigulova[2] and A. Urazalina[1,2,5]

[1]National Nanotechnology Laboratory of Open Type, Almaty, Kazakhstan
[2]Al-Farabi Kazakh National University, Almaty, Kazakhstan
[3]International Engineering Technological University, Almaty, Kazakhstan
[4]Fesenkov Astrophysical Institute, Almaty, Kazakhstan
[5]Institute of Nuclear Physics, Almaty, Kazakhstan
*e-mail: g_suliyeva@mail.ru

Radiative characteristics of accretion disks around rotating regular black holes

Abstract. Our research focuses on examining the characteristics of thin accretion disks encircling rotating regular black holes. In this study, we investigate the important features of accretion disks surrounding Bardeen's regular black holes, which play a crucial role in addressing the singularity issue. The horizon configuration of rotating Bardeen black holes is analyzed in details, as well as the innermost stable circular orbits related to this spacetime. The primary goal is to derive quantitively the radiative flux, differential and spectral luminosities of the accretion disk. Within the specified gravitational field, particularly, by taking the parameter $r_0^* > 0$ and fixing the $j = 0.2$, our findings show that the corresponding accretion disk's luminosity exceeds that one predicted by the Kerr metric at identical value of spin parameter ($j = 0.2$). Making the juxtaposition of Bardeen's black hole parameter r_0^* with the spin parameter j of the Kerr black hole we reveal that the spacetime corresponding to the non-rotating Bardeen black holes, in some certain cases, can imitate the Kerr spacetime.

Key words: rotating Bardeen spacetime, angular velocity, angular momentum, energy and radiative flux.

Introduction

One of general relativity's (GR) most intriguing predictions is the existence of black holes (BHs). Many observational data points available to us now support the presence of BHs in the universe [1, 2]. The existence of BHs in the universe has been overwhelmingly confirmed, and a new era of astronomical detection has begun with the inaugural detection of gravitational waves (GWs) originating from the binary BHs coalescence [3, 4] and the first images of the M87* and SgrA* shadows [1, 2]. Nevertheless, the interpretation of observations does not exclude alternative models of gravity.

A class of BHs with coordinate singularities (horizons) but without true singularities throughout spacetime are called regular black holes (RBHs). In most circumstances, determining a RBH often refers to a spacetime with finite curvature invariants everywhere, especially at the center of the BH [5, 6].

One of early goals for searching for RBH models was to eliminate spacetime singularities. Over the past few years, there has been a significant interest among scientists in singularity-free models of RBHs [7–10]. These models have gained attention because they offer an alternative to the complex causal structures that are inherent in BHs as predicted by GR.

Bardeen introduced the initial version of RBHs, now known as Bardeen BHs, by substituting the mass of Schwarzschild BHs with a function that depends on the radial distance. This modification eliminates the singularity of the Kretschmann scalar in the Bardeen BH. Additionally, the core of this BH exhibits de Sitter characteristics, meaning that the Ricci curvature is positive near the center of the BH [11]. Subsequently to this, several additional models for RBHs have been proposed in the literature [12–17]. It can be readily demonstrated that all of these alternative models for RBHs violate the strong

energy condition, thereby potentially challenging the singularity theorems. The effects of *static* Bardeen and Hayward RBHs on the spectral luminosity of accretion disks has been the subject of recent investigations, which have shown that these BHs behave differently from what is predicted for Schwarzschild and Kerr BHs [18].

Furthermore, the spectral and thermodynamic characteristics of accretion disks surrounding rotating Hayward BHs were studied by some of us in Ref. [19]. Additionally, employing the Hartle-Thorne geometry, we have analyzed the motion of test particles moving in circular orbits [20].

Motivated by the arguments stated above about RBHs, by examining the emission spectrum of the accretion disks, we set a goal to discern between rotating regular BHs and Kerr ones. The Novikov, Page, and Thorne models have been used to assess the properties of an accretion disk.

The paper is structured as follows: In Section II, we outline the key features of rotating RBHs and provide with the results concerning the motion of test particles in orbits encircled by accretion disks. In Section III, the thin accretion disk formalism is applied to considered model of RBHs. Lastly, our findings are discussed in Section V. Throughout the article, we adopt geometric units, where $G = c = 1$.

Bardeen regular black holes

The solution considered here is constructed on the basis of a mass function of the following form:

$$m(r) = M\left[1+\left(\frac{r_0}{r}\right)^q\right]^{-\frac{p}{q}}. \qquad (1)$$

The objective is to guarantee that the spacetime exhibits asymptotically flat behavior for positive values of p and q under static conditions. Prior research has indicated that such static solutions for RBHs can arise from a theory involving the coupling of nonlinear electrodynamics with gravity [21–23]. In this framework, M and r_0 denote the parameters for mass and length, respectively. The particular selections of $p = q = 3$ and $p = 3$, $q = 2$ correspond to Hayward [16] and Bardeen [11, 24] (BHs). Moreover, opting for $p \geq 3$ guarantees the smoothness of the geometry in the central region of static RBHs.

Upon deriving the aforementioned mass function, the more general line element, which accounts for the cosmological constant Λ and the Kerr rotation parameter will take the subsequent form in Boyer-Lindquist coordinates:

$$\begin{aligned} ds^2 = &-\frac{1}{\Sigma}\left(\Delta_r - \Delta_\theta a^2 \sin^2\theta\right)dt^2 + \\ &+\frac{\Sigma}{\Delta_r}dr^2 + \frac{\Sigma}{\Delta_\theta}d\theta^2 + \\ &+\frac{1}{\Xi^2\Sigma}\left[\left(r^2+a^2\right)^2\Delta_\theta - \Delta_r a^2\sin^2\theta\right]\sin^2\theta d\varphi^2 \\ &-\frac{2a}{\Xi\Sigma}\left[\left(r^2+a^2\right)\Delta_\theta - \Delta_r\right]\sin^2\theta dt d\varphi, \end{aligned} \qquad (2)$$

where

$$\Delta_\theta = 1+\frac{\Lambda}{3}a^2\cos^2\theta,\ \Sigma = r^2 + a^2\cos^2\theta, \qquad (3)$$

$$\Delta_r = \left(r^2+a^2\right)\left(1-\frac{\Lambda}{3}r^2\right) - 2rm,$$

$$\Xi = 1+\frac{\Lambda}{3}a^2, \qquad (4)$$

here a is the parameter of Kerr associated with the source's angular momentum. The metric (2) reduces to the Kerr solution when both Λ and r_0 are vanishing. Hereafter, we will consider the Bardeen rotating RBH for simplicity, i.e. with $p = 3$, $q = 2$, besides, without the cosmological constant, $\Lambda = 0$.

In Ref. [25], the authors investigated the event horizon of a rotating Bardeen BH surrounded by ideal liquid dark matter, and the BH as a particle accelerator. Also, the structure of the horizon and ergosphere in a rotating regular Bardeen BH was studied in Ref. [26].

The rotating Bardeen solution comprises inner and outer horizons, which are useful for defining the accretion disk's features and the values of j and r_0^*. The condition $1/g_{rr} = 0$ allows one to determine the horizons of rotating Bardeen BHs. The condition produces 10 roots, but only 4 of them are physically significant; the other 6 are not. The inner and outer horizons for Bardeen and Kerr BHs are given by two equations. Here, for rotating Bardeen BHs the outer and inner horizons are each given by two equations. The graphical representation of the inner and outer

horizons as functions of r_0^* and $j = a/M$ for rotating Bardeen BHs are shown in Figs. 1, 2, 3 and 4. In the limiting case, for vanishing j the horizon of the Bardeen BH is depicted by Fig. 3. Instead for vanishing r_0^* the horizon of the Kerr metric is described by Figs. 1 and 2.

Another straightforward representation of the horizons can be found using the same condition $1/g_{rr} = 0$, but here one should calculate r_0^* instead of r_h/M. In this case, we obtain two roots for r_0^* and keep only the positive one. The inner horizon r_h/M ranges from 0 to ~1 and the outer horizon varies from ~1 to 2 in analogy to Figs. 1, 2 and 3. The contours of fixed horizons are illustrated as functions of r_0^* and $j = a/M$ in Fig. 4. It turned out, that rotating Bardeen BHs indeed possess the two horizons as expected and there is no contradictions, which seem to appear in Figs. 1, 2 and 3.

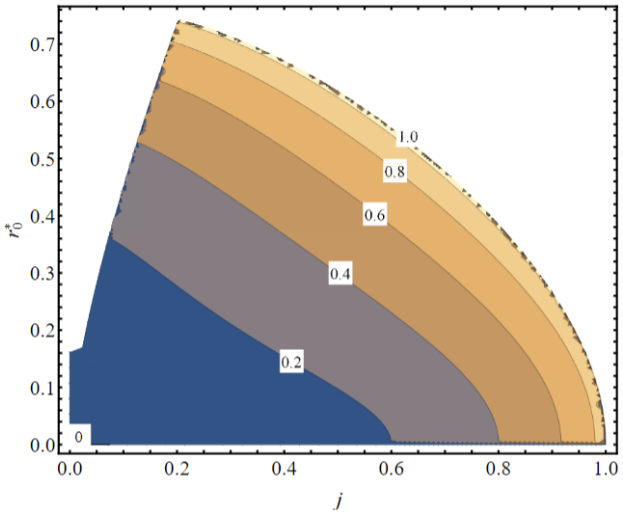

Figure 1 – Contour plots of the rotating Bardeen black hole's inner horizon positions as a function of the spin $j = a/M$ and deformation $r_0^* = r_0/M$ parameters. The numbers in the contours indicate the horizon radius normalized by the mass r_h/M

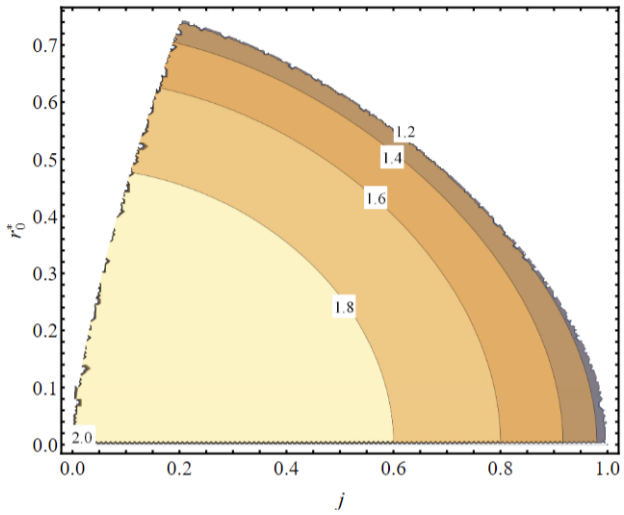

Figure 2 – Contour plots of the rotating Bardeen black hole's outer horizon positions as a function of $j = a/M$ and $r_0^* = r_0/M$. The numbers in the contours indicate the horizon radius normalized by the mass r_h/M

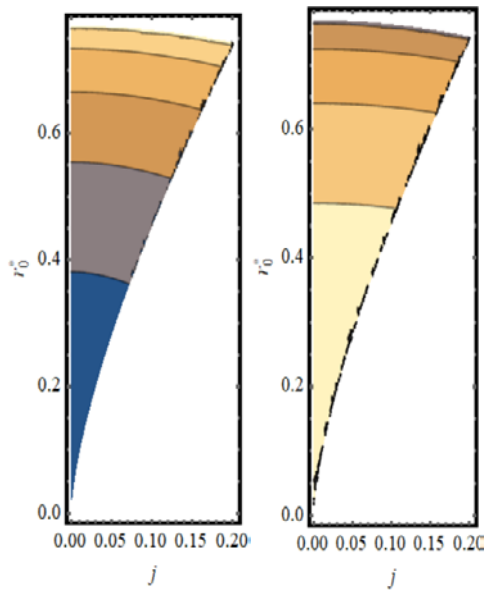

Figure 3 – Contour plots of the rotating Bardeen BH's inner (left panel) and outer (right panel) horizon positions as a function of $j = a/M$ and $r_0^* = r_0/M$. Contours indicate fixed values of r_h/M in analogy to Figs. 1 and 2

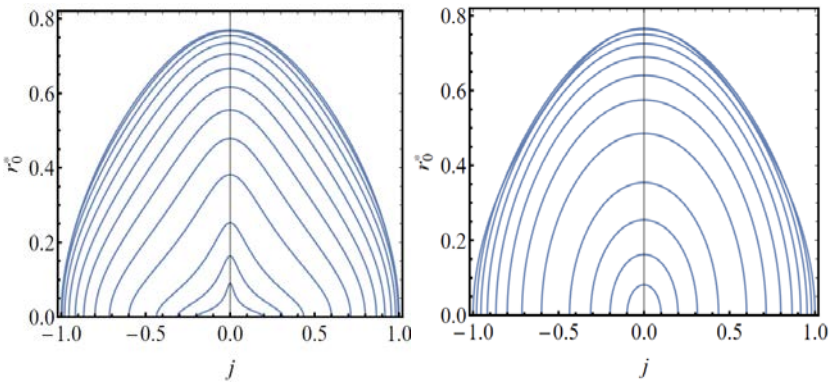

Figure 4 – Contour plots depict the positions of the inner (on the left panel) and outer (on the right panel) horizons of the rotating Bardeen BH depending on $j = a/M$ and $r_0^* = r_0/M$. The contours represent constant values of r_h/M

Circular orbits for massive test particles in the field of rotating Bardeen regular black holes

The angular velocity of test particles is obtained as follows:

$$\Omega = \frac{aM\left(r^2 - 2r_0^2\right) - \sqrt{M\left(r^2 - 2r_0^2\right)}(r^2 + r_0^2)^{5/4}}{a^2 M\left(r^2 - 2r_0^2\right) - (r^2 + r_0^2)^{5/2}}, \quad (5)$$

where $a > 0$ ($a < 0$) is the parameter related to the co-rotating (counterrotating) particles towards the BH's rotation direction.

Subsequently, the radial profiles for the angular momentum L and specific energy E are determined with the following expressions:

$$L = \frac{\left(Kr^2 + a^2\Pi_+\right)\Omega - aN}{\sqrt{K\left(\Pi_- + 2aN\Omega - \left(Kr^2 + a^2\Pi_+\right)\Omega^2\right)}}, \quad (6a)$$

$$E = \frac{\Pi_- + aN\Omega}{\sqrt{K\left(\Pi_- + 2aN\Omega - \left(Kr^2 + a^2\Pi_+\right)\Omega^2\right)}}, \quad (6b)$$

where

$$K = K(r) = (r^2 + r_0^2)^{3/2}, \quad (7)$$

$$N = 2Mr^2, \quad (8)$$

$$\Pi_+ = K + N, \quad (9)$$

$$\Pi_- = K - N. \quad (10)$$

The above expressions for angular momentum and specific energy are characterized by the RBH solution parameters, a and r_0, which fix the constants of motion at any given distance. Further, for the convenience of our analysis, dimensionless quantities are introduced, denoted as $\Omega^*(r) = M\Omega(r)$, $L^*(r) = L(r)/M$, $E^*(r) = E(r)$ and $r_0^* = r_0/M$. In Ref. [19] the behaviors of Ω^*, L^* and E^* are illustrated for Kerr BHs. As predicted, deviations from the Schwarzschild solution become more significant close to the BH (at smaller radial distance).

Massive test particles moving in the gravitational field of a compact object can have an innermost stable circular orbit (ISCO). The radius of the ISCO, denoted as r_{ISCO}, commonly marks the boundary of the accretion disk. This boundary is crucial as it signifies the closest stable orbit around the BH where matter can orbit without being drawn into it. Its specific numerical value is determined by various parameters that describe the gravity source, such as the mass, mass multipoles, angular momentum, charges and other parameters. The significance of the ISCO lies in its paramount role in the study of astrophysical compact objects. To make the constraints about the values for the source parameters, researchers can estimate the ISCO by studying the behavior of accretion disks. For instance, in the case of a Kerr BH, an estimation of the angular momentum may be obtained using an ISCO measurement, if an independent mass measure is available. The r_{ISCO} is determined by the condition $dL/dr = 0$ [27]. The r_{ISCO} for the Kerr spacetime is determined in Ref. [28]. However, the r_{ISCO} for Bardeen BHs cannot be obtained analytically. Consequently, the value of r_{ISCO} has been computed only numerically.

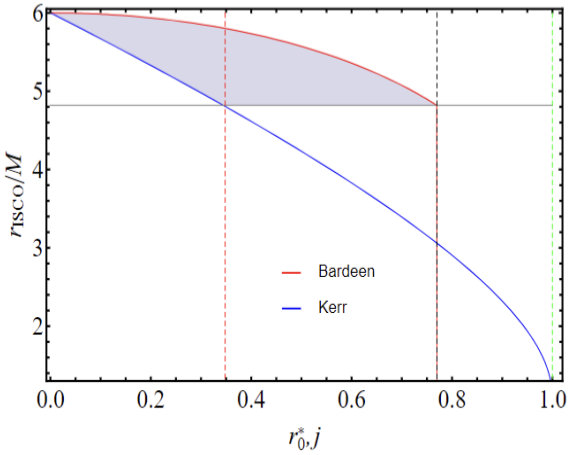

Figure 5 – The r_{ISCO} for the Bardeen BH versus r_0^* in comparison to the r_{ISCO} for the Kerr BH versus j. The shaded region shows the degeneracy in r_{ISCO} for both Bardeen and Kerr spacetimes

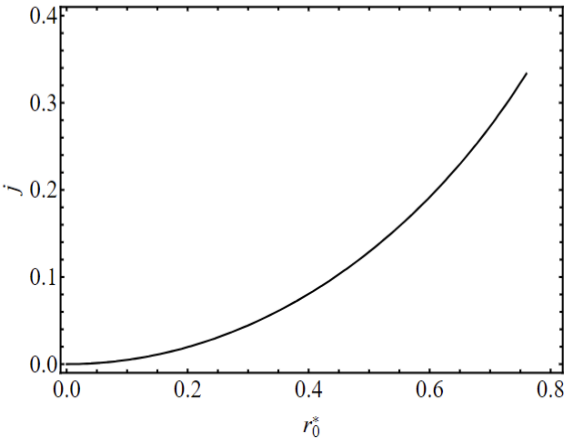

Figure 6 – Degeneracy in the r_{ISCO} values between the Bardeen and Kerr spacetimes.
This curve proves that the Bardeen BHs may mimic the Kerr BHs in particular cases.

Fig 5 depicts the r_{ISCO} in the Bardeen spacetime versus r_0^* in comparison to the r_{ISCO} of the Kerr metric versus dimensionless angular momentum *j*. The red and blue solid curves display the dependence of the r_{ISCO} versus *j*, r_0^* for Bardeen and Kerr BHs, respectively. The horizontal solid gray line and the shaded region show when r_{ISCO} is equal for both Bardeen and Kerr spacetimes. Thus, we may conclude that r_0^* of the Bardeen BH can mimic *j* of the Kerr BH up to $j \sim 3.5$. The degeneracy of the r_{ISCO} in the Bardeen spacetime versus r_0^* and that one for the Kerr metric as a function of *j* is displayed in the Fig. 6.

Thin accretion disk spectra

We employ the well-known formalism outlined in the pioneering works of Page and Thorne, and Novikov and Thorne [29, 30]. Our goal is to understand the dynamics of the accretion disk surrounding spinning RBHs, using numerical analysis.

The radiative flux $\mathcal{F}$ is determined as follows:

$$\mathcal{F}(r) = -\frac{\dot{\mathrm{m}}}{4\pi\sqrt{-g}} \frac{\Omega_{,r}}{(E-\Omega L)^2} \int_{r_{\mathrm{ISCO}}}^{r} (E-\Omega L) L_{,\tilde{r}} d\tilde{r}\,, \tag{11}$$

where $\dot{\mathrm{m}}$ is the mass accretion rate and $\sqrt{-g} = \sqrt{-g_{rr}\left(g_{tt}g_{\varphi\varphi} - g_{t\varphi}^2\right)}$.

In this context, the assumption of an accretion disk in thermodynamic equilibrium is another crucial approximation. On this supposition, it is possible to describe the radiation coming from the disk itself as isotropic radiation from a black body. It is possible to compute the temperature related to this radiation by applying the Stefan-Boltzmann formula

$$\mathcal{F}(r) = \sigma T^{*4}, \tag{12}$$

here the radiative flux, which is a function of radial distance and denoted by $\mathcal{F}(r)$ and σ is the Stefan-Boltzmann constant.

The differential luminosity $\frac{d\mathcal{L}_\infty}{d\ln r}$ can be calculated from the flux $\mathcal{F}$ using the following relationship

$$\frac{d\mathcal{L}_\infty}{d\ln r} = 4\pi r\sqrt{-g}E\mathcal{F}\,(r). \tag{13}$$

Radiation released by the accretion disk at a certain distance *r* is described by the differential luminosity and the radiative flux. In real-world observations, the frequency and the spectral distribution are physically quantifiable variables and prove to be easier to measure.

The spectral luminosity $\mathcal{L}_{\nu,\infty}$ is defined as follows:

$$\nu\mathcal{L}_{\nu,\infty} = \frac{60}{\pi^3}\int_{r_{ISCO}}^{\infty} \frac{\sqrt{-g}E}{M_T^2} \frac{(u^t y)^4}{\exp[u^t y/\mathcal{F}^{*1/4}]-1} dr\,, \tag{14}$$

here $y = h\nu/kT^*$, with h, k and ν representing the Planck's constant, Boltzmann constant and frequency at which the radiation is emitted. Given the above, u^t can be defined as

$$u^t(r) = \frac{1}{\sqrt{-g_{tt} - 2\Omega g_{t\varphi} - \Omega^2 g_{\varphi\varphi}}}. \tag{15}$$

Results and discussion

Figs. 7, 8 illustrate orbital angular velocity of the test particles $\Omega^*(r)$ versus normalized radial distance *r/M*. Fig. 7 displays the results for a rotating Bardeen BH with various values of $j = [0, 0.2, 0.4, 0.6, 0.8]$ at a fixed r_0^* =0.2. In comparison to the static Bardeen spacetime (black solid color) with *j* = 0.2, the rotating Bardeen spacetime with the varying values of *j* at fixed r_0^* =0.2 lead to a smaller angular velocity in all ranges of *r*. The Fig. 8 shows the results for different values of $r_0^* = [0, 0.25, 0.5, 0.75]$ at a fixed *j* = 0.2. The solid black curve indicates the Kerr metric. The angular

velocity in Kerr spacetime with r_0^* =0 at fixed j=0.2 is greater than the rotating Bardeen spacetime in all ranges of r.

In Figs. 9, 10 we depicted the dependence of L^* on the r/M for rotating Bardeen BHs with various values j at fixed r_0^* =0.2 (Fig. 9) and with various values of r_0^* at fixed j = 0.2 (Fig. 10).

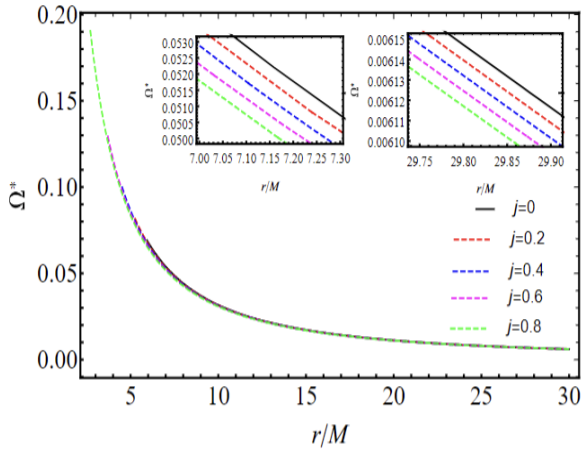

Figure 7 – Dependence of test particle's angular velocity on the radial distance r/M for rotating Bardeen BHs with r_0^* =0.2

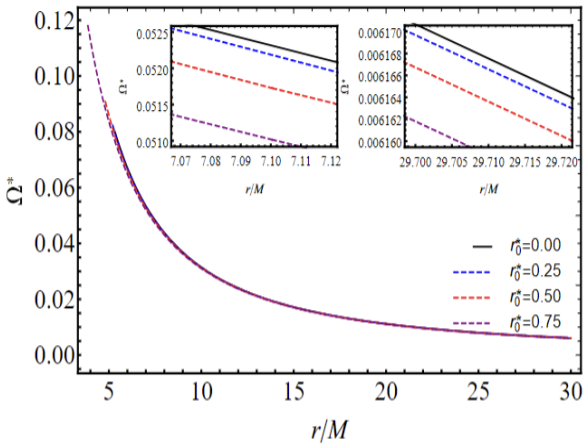

Figure 8 – Dependence of test particle's angular velocity on the radial distance r/M for rotating Bardeen BHs with j = 0.2

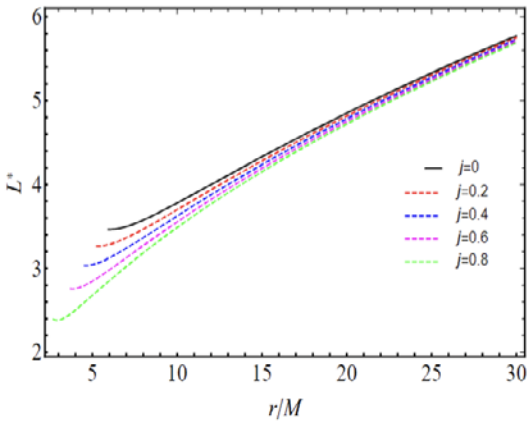

Figure 9 – L^* as a function of r/M for rotating Bardeen BHs with r_0^* =0.2

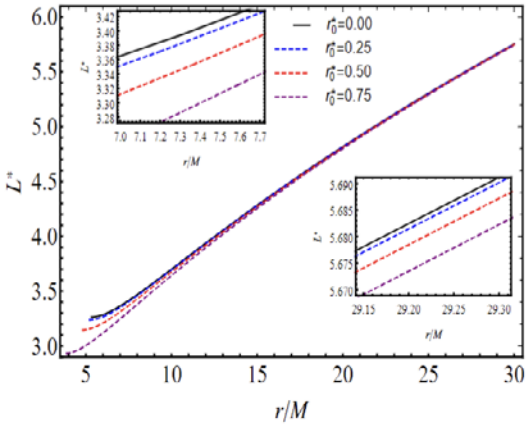

Figure 10 – L^* as a function of r/M for rotating Bardeen BHs with j = 0.2

In Figs. 11, 12 we constructed the dependence of E^* of test particles on the r/M for rotating Bardeen BHs with various values j at fixed r_0^* =0.2 (Fig. 11) and with various values of r_0^* at fixed j = 0.2 (Fig. 12).

As seen from Figs. 8, 10, 12 $\Omega^*(r)$, $L^*(r)$, E^* with varied values of r_0^* at fixed j are always less than the Kerr case (black solid curve). In Figs. 7, 9, 11 $\Omega^*(r)$, $L^*(r)$, E^* with different values of j at fixed r_0^* are always less than in case static Bardeen BH (black solid curve).

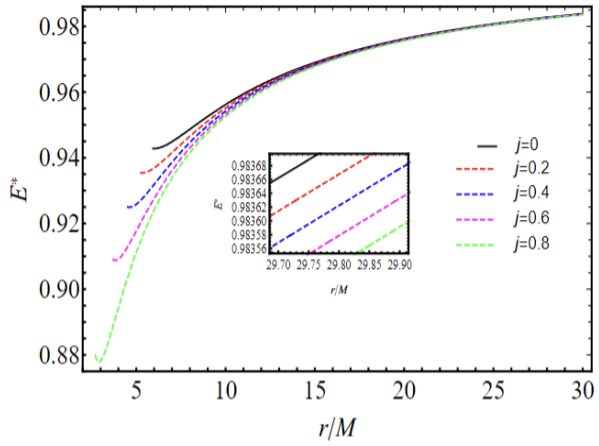

Figure 11 – E^* as a function of r/M for rotating Bardeen BHs with r_0^* =0.2

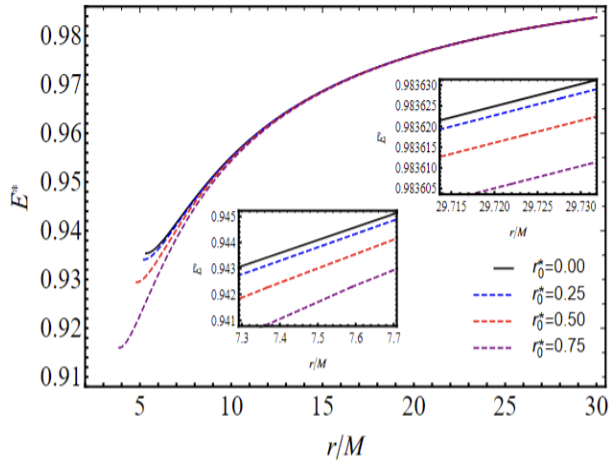

Figure 12 – E^* as a function of r/M for rotating Bardeen BHs with j = 0.2

It is worth mentioning that we normalized the flow by dividing it by the total BH mass M in order to maintain the dimensionless argument of the exponential term. Furthermore, a new quantity $\mathcal{F}^*(r)$, is determined as: $\mathcal{F}^*(r) = M^2\mathcal{F}(r)$. This normalization ensures that the flux is represented consistently in the computations that follow.

Figs. 13, 14 show the $\mathcal{F}(r)$ for the rotating Bardeen BHs. We left j arbitrary and set r_0^* =0.2 (Fig. 13) and we fixed j = 0.2 and let r_0^* to vary (Fig. 14). The flux for the spinning Bardeen BHs with j = 0.2 and $r_0^* > 0$ is larger than in the Kerr metric case. The Fig. 13 illustrates how the flux grows in accordance with the chosen values of j. The $\mathcal{F}(r)$ for the spinning Bardeen BHs (r_0^* =0.2j = 0.2) is greater than that in the static Bardeen spacetime case.

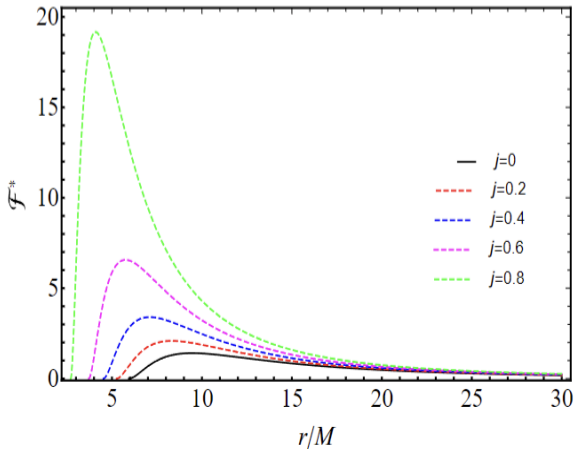

Figure 13 – Radiative flux F^* multiplied by 10^5 of the accretion disk versus normalized radial distance r/M for rotating Bardeen BHs with r_0^* =0.2

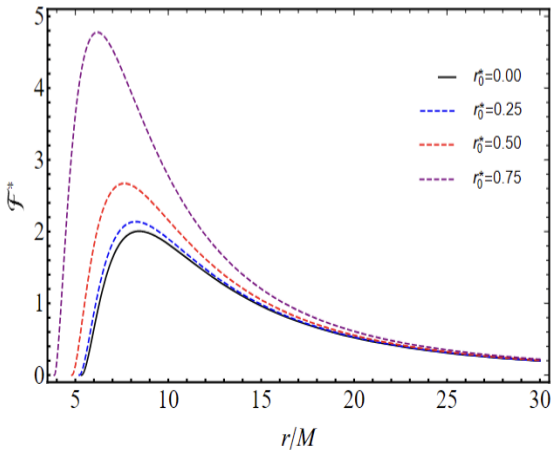

Figure 14 – Radiative flux F^* multiplied by 10^5 of the accretion disk versus normalized radial distance r/M for rotating Bardeen BHs with j = 0.2

The dimensionless temperature T^* of accretion disks for spinning Bardeen BHs spacetime with $j = [0, 0.2, 0.4, 0.6, 0.8]$ at fixed r_0^* =0.2 and $r_0^* = [0, 0.25, 0.5, 0.75]$ at fixed j = 0.2 is presented in Figs. 15 and 16, respectively. The temperature T^* for the rotating Bardeen spacetime is always larger than in the static Bardeen spacetime (Fig. 15). Fig. 16 illustrates that the temperature is permanently greater than in the Kerr spacetime for values of r_0^*=[0.25, 0.5, 0.75].

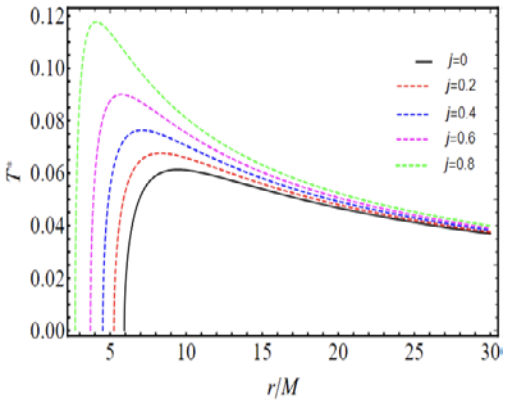

Figure 15 – The accretion disks' temperature T^* around the rotating Bardeen BHs with r_0^* =0.2

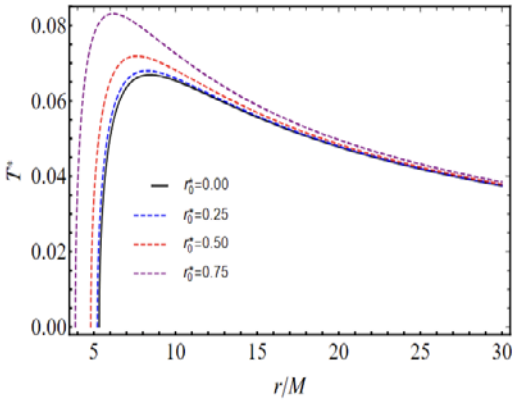

Figure 16 – The accretion disks' temperature T^* around the rotating Bardeen BHs with j = 0.2

Differential luminosity versus the r/M for the rotating Bardeen BH with $j \geq 0$ at fixed r_0^* =0.2 and $r_0^* \geq 0$ at fixed j = 0.2 is shown in Figs. 17 and 18, respectively. The behavior of the differential luminosity is similar to the radiative flux displayed in Figs. 13 and 14. It has to do with the fact that Eq. (13) relates both quantities.

The spectral luminosity $\mathcal{L}_{\nu,\infty}$, as determined by Eq. (14), is illustrated in Figs. 19 and 20 versus $h\nu/kT^*$ (as in previous cases, the fixed r_0^* =0.2 (Fig.19), and fixed j = 0.2 (Fig. 20)). The effect of angular momentum is that the spectral luminosity at higher values of j is superior. A similar trend is observed in the case when the values of r_0^* increase for a fixed j. For both considered variations, the influence of rotation and length parameter is more evident with the growth of frequency at which the light is emitted. The spectral luminosity, as seen in Fig. 20, is smaller the whole ranges around the Kerr BHs with respect to the rotating Bardeen BHs.

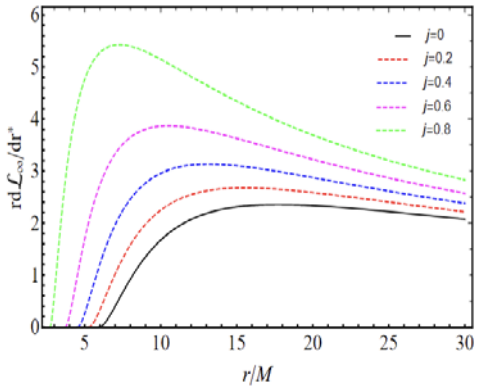

Figure 17 – The accretion disks' differential luminosity multiplied by 10^2 versus of r/M for rotating Bardeen BHs with r_0^* =0.2

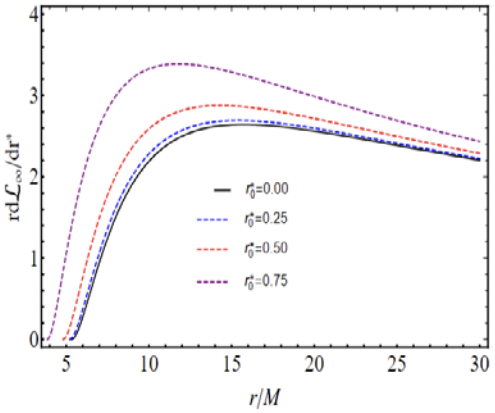

Figure 18 – The accretion disks' differential luminosity multiplied by 10^2 versus of r/M for rotating Bardeen BHs with j = 0.2

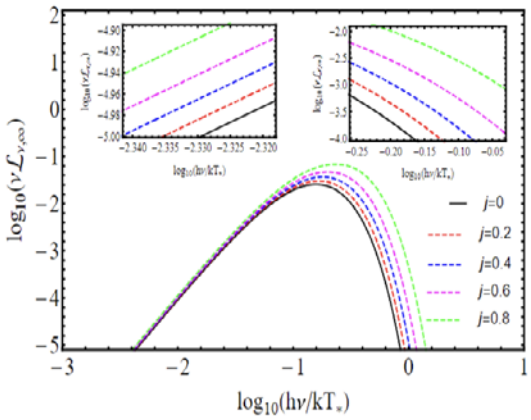

Figure 19 – Spectral luminosity versus the accretion disk's black-body emission frequency for rotating Bardeen BHs with r_0^* =0.2

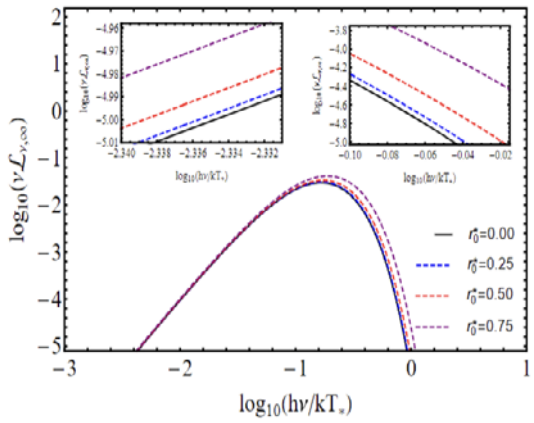

Figure 20 – Spectral luminosity versus the accretion disk's black-body emission frequency for rotating Bardeen BHs with $j = 0.2$

Final outlooks and perspectives

We used accretion disk luminosity to distinguish different types of spacetime that model BH or BH mimickers. Here, we investigated what kinds of effects are anticipated from rotating RBH solutions in the absence of a cosmological constant. We thus emphasized the capability of distinguishing rotating Bardeen BH from Kerr spacetime. For example, by analyzing the structure of horizons and values of r_{ISCO}, it is possible to show that the Kerr BHs are conceptually different from the Bardeen BHs.

The neutral test particle behaviors in the circular geodesics were calculated. Here we have explored the Novikov-Thorne-Page model of the thin accretion disk. Regarding this, we assessed the radius of ISCO, radiative flux, differential and spectral luminosities. Particularly, our results demonstrate that the luminosity for rotating Bardeen BHs is greater than for Kerr spacetime with fixed spin parameter $j = 0.2$. This peculiarity can serve as a means to differentiate between the two spacetimes.

The observed higher luminosity in the case of rotating Bardeen BHs suggests that these systems possess inherent characteristics that promote more efficient energy release and radiation emission compared to their Kerr counterparts at fixed $j = 0.2$. One plausible explanation for this phenomenon lies in the distinct nature of the spacetime geometry described by the Bardeen metric. Unlike Kerr spacetime, which is governed solely by the mass and spin of the black hole, the Bardeen metric incorporates additional parameter that can influence the gravitational dynamics near the BH.

Furthermore, the discrepancy in luminosity between Bardeen and Kerr BHs highlights the importance of considering alternative BH models beyond the traditional Kerr paradigm. It suggests that the specific geometric properties and underlying physics encoded in alternative BH metrics can significantly impact the observational signatures of accretion disks.

Lastly, we showed that there is the degeneracy in r_{ISCO} between the Bardeen and Kerr BHs. We explicitly demonstrated that the Bardeen metric can mimic the effects in the Kerr metric related to the r_{ISCO} up to the values of $j = 0.35$. Hence, this argument can also be used to distinguish the two spacetime.

It would be interesting to study radiative characteristics of other spacetimes in alternative, extended and modified theories of gravity. It is planned to consider this issue in future works.

Acknowledgments

YeK acknowledges Grant No. AP19575366, TK acknowledges the Grant No. AP19174979, GS acknowledges Grant No. AP19680128, AU acknowledges Grant No. BR21881941 from the Science Committee of the Ministry of Science and Higher Education of the Republic of Kazakhstan.

References

1. The Event Horizon Telescope Collaboration "First M87 Event Horizon Telescope Results. I. The Shadow of the Supermassive Black Hole." *The Astrophysical Journal Letters* 875, No. 1 (2019): 1–17.
2. Akiyama K. et al. (Event Horizon Telescope) "First Sagittarius A* Event Horizon Telescope Results. I. The Shadow of the Supermassive Black Hole in the Center of the Milky Way." *The Astrophysical Journal Letters* 930, No. 2 (2022): 1–21.
3. Abbott B.P. et al. "Observation of gravitational waves from a binary black hole merger." *Physical Review Letters* 116, No. 6 (2016): 1–7.
4. Abbott B.P. et al. "GW151226: Observation of Gravitational Waves from a 22-Solar-Mass Binary Black Hole Coalescence." *Physical Review Letters* 116, No. 24. (2016): 1–14.
5. Dymnikova I. "Vacuum Nonsingular Black Hole." *General Relativity and Gravitation* 24, No. 3 (1992): 235–242.
6. Bronnikov K.A. "Regular magnetic black holes and monopoles from nonlinear electrodynamics." *Physical Review D* 63, No. 4 (2001): 1–6.

7. Melgarejo G., Contreras E. and Bargueno P. “Regular black holes with exotic topologies.” *Physics of the Dark Universe* 30, No. (2020): 1–7.
8. Bambi C. “Regular Black Holes: Towards a New Paradigm of Gravitational Collapse” doi:10.48550/arXiv.2307.13249, 2307.13249.
9. Lan C., Yang H., Guo Y. and Miao Y.-G. “Regular black holes: A short topic review.” *International Journal of Theoretical Physics* 62, No. 9 (2023): 202–247.
10. Sebastiani L. and Zerbini S. “Some remarks on non-singular spherically symmetric space-times.” *Astronomy* 1, No. 2 (2022): 99–125.
11. Bardeen J.M. “Non-singular general relativistic gravitational collapse.” in *Proceedings of the International Conference GR5* 174, No. 1 (1968): 174.
12. Bogojevic A. and Stojkovic D. “A Non-Singular Black Hole.” *Physical Review D* 61, No. 8 (2000): 1–11.
13. Toshmatov B., Ahmedov B., Abdujabbarov A. and Stuchlık, Z. “Rotating regular black hole solution.” *Physical Review D* 89, No. 10 (2014): 1–8.
14. Ghosh S.G., Maharaj S.D. “Radiating Kerr-like regular black hole” *European Physical Journal C* 75, No. 7 (2015): 1-7.
15. Azreg-Aınou M. “Generating rotating regular black hole solutions without complexification.” *Physical Review D* 90, No. 6 (2014): 1–13.
16. Hayward S.A. “Formation and evaporation of non-singular black holes.” *Physical Review Letters* 96, No. 3 (2006): 1–4.
17. Bambi C. and Modesto L. “Rotating regular black holes.” *Physics Letters B* 721, No. 4-5 (2013): 329–334.
18. Akbarieh A.R., Khoshragbaf M. and Atazadeh, M. “Accretion disk around regular black holes.” 10.48550/arXiv.2302.02784, (2023): 1–12.
19. Boshkayev K., Konysbayev T., Kurmanov Ye., Luongo O., Muccino M., Taukenova A. and Urazalina A. “Luminosity of accretion disks around rotating regular black holes.” *European Physical Journal C* 84, No. 3 (2024): 1–12.
20. Boshkayev K., Konysbayev T., Kurmanov Ye., Luongo O., Muccino M., Quevedo H. and Urazalina A. “Accretion disk in the Hartle-Thorne spacetime.” *European Physical Journal Plus,* 124, No. 273, (2024): 1–17.
21. Ayon-Beato E. and Garcia A. “Regular Black Hole in General Relativity Coupled to Nonlinear Electrodynamics.” *Physical Review Letters* 80, No. 23 (1997): 5056–5059.
22. Bronnikov K.A. “Comment on “Regular Black Hole in General Relativity Coupled to Nonlinear Electrodynamics.” *Physical Review Letters* 85, No. 21 (2000): 4641.
23. Bronnikov K.A. “Regular black holes sourced by nonlinear electrodynamics.” arXiv:2211.00743, (2022): 1–30.
24. Ansoldi S. “Spherical black holes with regular center: a review of existing models including a recent realization with Gaussian sources.” arXiv:0802.0330, (2008): 1–36.
25. Li Q.-Q., Zhang Y., Li Q. and Sun Q. “Rotating Bardeen black hole surrounded by perfect fluid dark matter as a particle accelerator.” *Communications in Theoretical Physics* 75, No. 10 (2023):1–10.
26. Ghosh S.G. and Amir M. “Horizon structure of rotating Bardeen black hole and particle acceleration.” *European Physical Journal C* 75, No. 11 (2015): 1 – 12.
27. Boshkayev K., Gasperin E., Gutierrez-Pineres A.C., Quevedo H. and Toktarbay S. “Motion of test particles in the field of a naked singularity.” *Physical Review D* 93, No. 2 (2016): 1–16.
28. Boshkayev K., Konysbayev T., Kurmanov E., Luongo O., Malafarina D. and Quevedo H. “Luminosity of accretion disks in compact objects with a quadrupole.” *Physical Review D* 104, No. 8 (2021): 1–10.
29. Novikov I.D. and Thorne K.S. “Astrophysics of black holes.” Black Holes (Les Astres Occlus), 343–350.
30. Page D.N. and Thorne K.S. “Disk-Accretion onto a Black Hole. Time-Averaged Structure of Accretion Disk.” *The Astrophysical Journal* 191, No. 2 (1974): 499–506.

Information about authors:
Kurmanov Yergali – PhD, Acting Associate Professor at Al-Farabi Kazakh National University, Almaty, Kazakhstan, e-mail: ergaly_90@mail.ru
Konysbayev Talgar – PhD at Al-Farabi Kazakh National University, Almaty, Kazakhstan, e-mail: talgar_777@mail.ru
Suliyeva Gulnara (corresponding author) – 2nd year doctoral student at the Department of Theoretical and Nuclear Physics at Al-Farabi Kazakh National University, Almaty, Kazakhstan, e-mail: g_suliyeva@mail.ru
Gulfeiruz Ikhsan – Junior Research Associate at National Nanotechnology Laboratory of Open Type, Almaty, Kazakhstan, e-mail: gulfeyruz.ihsan@mail.ru
Nazym Saiyp – 1st year master student at the Department of Solid State Physics and Nonlinear Physics at at Al-Farabi Kazakh National University, Almaty, Kazakhstan, e-mail: nazymsaiyp1@gmail.com
Guldana Rabigulova – 1st year master student at the Department of Solid State Physics and Nonlinear Physics at at Al-Farabi Kazakh National University, Almaty, Kazakhstan, e-mail: guldanaberikhanovna@gmail.com
Ainur Urazalina – PhD, Senior Lecturer at Al-Farabi Kazakh National University, Almaty, Kazakhstan, e-mail: y.a.a.707@mail.ru

Received 03 April 2024
Accepted 26 May 2024